Detailed Successive Layer Modeling and Design Factor Analysis for Single Micro-LED Pixel

Chung-Jen Ou, Kai-Ping Chang, Ming-Wei Tasi, Chien-Chih Chen, Yu-Min Chen, Chih-Wei Lo, and Dong-Sing Wuu, *Senior Member, IEEE*

***Abstract*—The major factors associated with the manufactured structures and photon emission intensity distribution must be accurately identified for the complicated optical design parameters associated with micro-LED pixels. This study presents the methodologies and reveals the sequential calculating protocol in each layer for pixel-level optical simulations, based on which the boundary condition errors associated with common optical simulations can be corrected. Moreover, the optical effect on each epitaxial layer of the micro-LED design is revealed, and the rationality of the setting of the finite-radius receiver with a pseudo-extended substrate material is also explained with respect to the intrinsic and extrinsic pixel-intensity distribution properties. Finally, the design of experiments DOE L_{18} orthogonal array table is demonstrated by the Taguchi method to explore the principal factors for the parameter design of the micro-LED layers. The results indicate that the sapphire thickness, the P-GaN layer, the buffer layers, and an additional substrate plate are the four significant factors that primarily influence the luminous power and the corresponding uniformity on the exit pupil of micro-LEDs. Based on the luminous power uniformity, the signal-to-noise ratio in the sapphire thickness is 16.9, and the extended substrate plate is 9.8, which is $\sim$10 times $>$ the interaction design parameter, such as the etching angle and reflective index of the extended substrate of the micro-LED pixel. These specific design factors can be the major optimization parameters for cost control and performance improvement.**

***Index Terms*—Micro-LED pixel, taguchi method, ray-tracing program, boundary conditions, DOE method, far-field receiver.**

Manuscript received 24 October 2022; accepted 27 October 2022. Date of publication 2 November 2022; date of current version 16 November 2022. This work was supported in part by Coretronic, Taiwan, under Grant RT01-2021070119, in part the Ministry of Science and Technology, Taiwan under Grants 108-2221-E-005-072-MY3, 108-2811-E-005-512-MY3, 108-2221-E164-002, 110-2218-E-A49-012-MBK, and 111-2218-E-A49-019-MBK, and in part by the Innovation and Development Center of Sustainable Agriculture from the Featured Areas Research Center Program through the Higher Education Sprout Project by the Ministry of Education (MOE), Taiwan. *(Corresponding authors: Dong-Sing Wuu; Kai-Ping Chang.)*

Kai-Ping Chang and Chih-Wei Lo are with the Department of Materials Science and Engineering, National Chung Hsing University, Taichung 40227, Taiwan (e-mail: a3322123@dragon.nchu.edu.tw; g109066109@mail.nchu.edu.tw).

Chung-Jen Ou, Ming-Wei Tasi, and Chien-Chih Chen are with the Coretronic Corporation, Hsinchu 30078, Taiwan (e-mail: crou@hust.edu.tw; richard.tsai@coretronic.com; jeffcc.chen@coretronic.com).

Yu-Min Chen is with the Coretronic Corporation, Hsinchu 30078, Taiwan, also with the Department of Photonics, National Yang Ming Chiao Tung University, Hsinchu 30010, Taiwan (e-mail: jabby0317.eo08g@nctu.edu.tw).

Dong-Sing Wuu is with the Department of Applied Materials and Optoelectronic Engineering, National Chi Nan University, Nantou 54561, Taiwan, also with the Department of Materials Science and Engineering, National Chung Hsing University, Taichung 40227, Taiwan, and also with the Innovation and Development Center of Sustainable Agriculture, National Chung Hsing University, Taichung 40227, Taiwan (e-mail: dsw@ncnu.edu.tw).

Digital Object Identifier 10.1109/JPHOT.2022.3218765

I. Introduction

MICRO-LEDs are essential for new-generation displays and biomedical device applications [1], [2]. Designing high-efficiency micro-LEDs is the central dogma of these specific applications due to the portability and lightweight requirements. Taking the extended reality (XR) system as an example, smaller pixel size, higher resolution, and a single panel solution with full-color conversion schemes are the major trends of the current research direction and market [3], [4], [5]. Thus, the need arises for a detailed analysis procedure for pixel-based intensity distribution (apodization), light extraction, and uniformity predictions. Among various reports, few studies have discussed the optical modeling of the construction and design of micro-LED devices [6], [7], [8]. However, there is a lack of simulation details and a proper protocol for further investigation. A possible improvement protocol for micro-LED pixel reduction simulation is still insufficient.

Generally, a computational method is essential to overcome the various configurations for the novel design of micro-LED pixel structures. Thus, identifying an appropriate modeling tool at the pixel level is critical before fabrication. Although the geometric ray-tracing assumption has been introduced for pixel size simulation [6], [7], the maintenance of the privilege and effectiveness criteria should be considered. It is rational to examine the assumption as well as the corresponding boundary and interface conditions for these pixels and subpixel calculation scenarios in advance. Thus, this study aims to introduce appropriate modeling procedures and demonstrate strategies for identifying the major forming factors of micro-LED pixel structures. These strategies can provide an adequate model for estimating the micro-LED efficiency. Based on successive layer modeling, the key factors associated with pixel performance can be clearly identified. Thus, the design of highly efficient color conversion schemes when considering structures in the pixel recycle chamber can be considerably improved [9] (*e.g.*, photons bouncing between bandpass filters for quantum dots or various spectra of exciting material).

II. Experimental Procedure

A. Modeling Problems

The ray-tracing program is the rational choice to proceed with the micro-LED pixel simulation. However, for the high-resolution pixels with downsizing demands, the effectiveness of employing the geometric ray-tracing algorithm is an issue. Another concern is the photon trajectory, with the interface

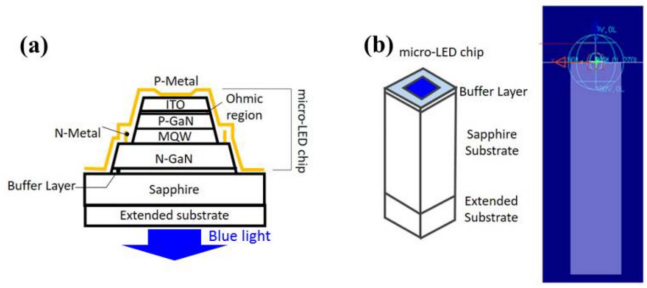

Fig. 1. (a) Fifty-micrometer micro-LED from NCHU [6], and (b) Tube-like model.

feasibility by Snell's law after the epitaxial process. Here the Fresnel number is introduced as a possible indicator to examine the rationality of the geometric ray tracing in the pixel-level simulation.

$$F = \frac{W^2}{L \cdot \lambda} \tag{1}$$

Here, W is the exit pupil or micro-LED, L is the characteristic propagation length (the radius of the receiver will be discussed in detail later), and λ is the wavelength. Consider a micro-LED pixel structure [6] (Fig. 1(a)) with $W = 50$ um and $L = 575$ um sapphire thickness. The structures comprise sapphire, the buffer layer, N-GaN layer, multi-quantum well (MQW), P-GaN layer, Ohmic region, and indium tin oxide (ITO), with metal layers as the reflective surface and conducting layers.

The sapphire substrate is removed from most micro-LED chips. However, the transfer technique with sapphire substrate might be useful for color-covered full-color micro-LED display. This is integrated with the quantum dot photoresist (QDPR) on the micro-LED display and distributed Bragg reflector deposited on sapphire [6], [10]. Further, the substrate might be suitable for the back-end process to offset the bending stresses caused by the differential thermal expansion of the substrate and epilayer [11].

For a micro-LED with a 450-nm wavelength, the Fresnel number (F) is $\sim$13. Although F is not strictly $>>1$ [12], this proves that geometric ray tracing (now photon tracing) is an acceptable evaluation tool. Then, the boundary conditions and receivers (detectors) for building the pixel-based optical model are considered. Due to the operating protocol, the conventional method might naturally lead to the usage of a finite-region "substrate tube" with an interface between environments (mainly air). Fig. 1(b) presents an example and assigns a far-field receiver to estimate the intensity distributions. However, the problem stems from the resulting inaccurate boundary conditions (artificial refracting interface) between the pixels and the false side wall effects since the real scenario is that the photons must remain to propagate in the true substrate size.

For a single micro-LED die, the boundary condition encounters discontinuity with respect to the material properties, which is quite difference in case of a micro-LED array. For example, mass transfer technology is required to prepare and cut the red, green, and blue chips on the display substrate for manufacturing color micro-LEDs [13]. Under this condition, the boundary conditions (air and sapphire) of the substrate can be described directly based on the conventional setting of the optical simulation software.

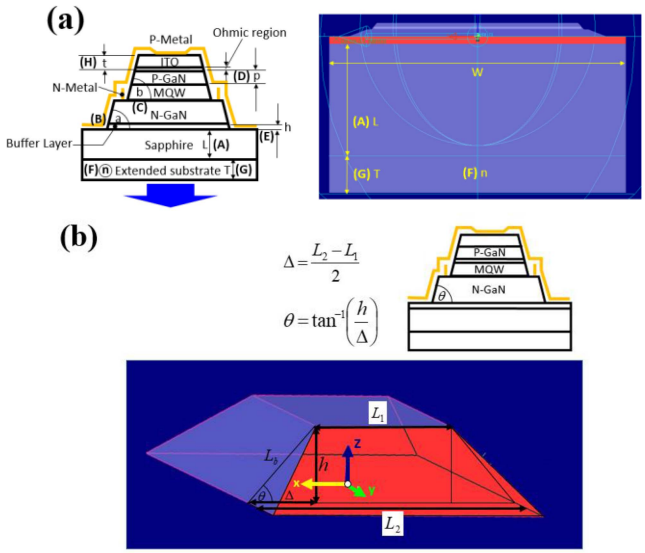

Fig. 2. (a) (A) Sapphire thickness (L) = 570 um, (B) N-GaN layer etching angle (a) = 21.8°, (C) Etching angle of the MQW/P-GaN/ITO compound (b) = 48.9°, (D) P-GaN layer thickness (p) = 0.4 um, (E) Buffer layer thickness (h) = 1.55 um, (F) Extended substrate refractive index (n) = 1.57, (G) Extended substrate thickness (T) = 5 um, and (H) ITO thickness (t) = 0.28 um. Notations A–H also represent the design of the experimental factors in the latter section, with a 1.42-um constant thick N-GaN layer. (b) Definition of taper ratio (ε) = L_1/L_2.

However, the micro-LED dies are assembled in an array for more practical scenario. Consequently, modeling the appropriate boundary conditions for a single pixel is essential.

B. Modeling Strategies

To build an appropriate modeling protocol, this subsection discusses the modeling strategy formation for pixel-based simulations.

1) Construction of Successive Layer Model: Fig. 2(a) shows the layer structures of the demonstrated 50-μm blue micro-LED [6]. The modeling of the etching angle was performed by assigning a taper ratio ε between the bottom and top surfaces. By observing the cross-section view, the area relationship between the bottom surface, top surface, layer thickness, and etching angle is described in Fig. 2(b).

The successive building of the LED layers of this model is explained as follows. Each layer comprises six surfaces: the top, bottom, and four side surfaces. The top surface interface of a specific layer meets the continuity condition with the bottom surface of the other epitaxial layer. To manage this, a pixel model must activate the continuity options between the layer interfaces (*e.g.*, "glue," "adhesive," or "cement"). For illustration, the top and bottom surfaces of the MQW layer were cemented to the P-GaN bottom and N-GaN top surfaces, respectively. The four side surfaces of the MQW layer were set as the capability for the TIR surface if the criterion was satisfied (denoted as the TIR surface for short). According to the micro-LED design shown in Fig. 2(a), the four sides are coated with a metal layer, ensuring photon reflection. This cement procedure is repeated along with adjusting the layer coordinates carefully. Fig. 3 shows a clear successive construction procedure of the micro-LED model with

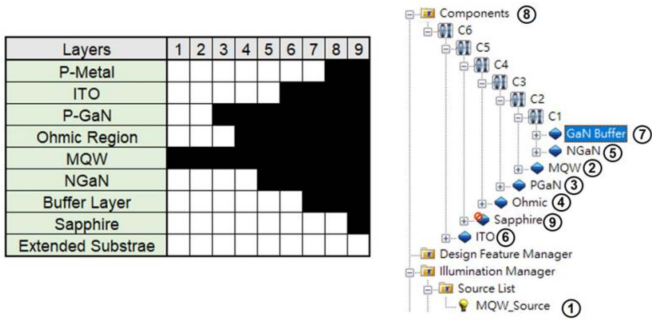

Fig. 3. Successive construction of micro-LED layers.

the corresponding layer relationship in the optical software. The "+" notation indicates the cement process between the micro-LED layers.

As the electron and holes recombine in the MQW layer, the generated photons emit as a Lambertian source in all directions. The photon emission moves toward the top direction, through the P-GaN and ITO layers, and is reflected by the metallic layer. Afterward, the photons pass through the ITO layer, P-GaN layer, MQW, N-GaN layer, buffer layer, and sapphire substrate (extended material) and leave the micro-LED pixel structure. In contrast, photons can also reach directly from the MQW through the substrate, N-GaN layer, buffer layer, and sapphire substrate and leave the micro-LED. The classical Snell law is dominated between the interface under the present surface conditions and the Fresnel number. Thus, the TIR phenomenon is one of the ratiocinations.

2) MQW Layer: Assigning the MQW electron–hole recombination zone as a volumetric photon source is reasonable. However, note that two entities should be modeled in the MQW layer simultaneously: the MQW-emitting region (light source) and layer (layer entity). The MQW-emitting region is immersed inside an MQW layer with the same refractive index (n) as GaN. The algorithm without this immersion setting fails during the micro-LED simulation due to incorrect photon propagation inside the MQW layer.

The n-value of the emitting region (photon source) is assigned to the GaN material, and it is immersed in the MQW layer with the same n-value. This approach ensures the continuity of the material properties between the P-GaN and N-GaN layers. Also, it naturally provides the proper boundary conditions between the P-GaN layer, the MQW-emitting regional interfaces, the MQW layer, and the N-GaN layer. The only glitch is that the emitting region has an imperfect geometric shape. This shape should be measured by the instrument, and then a nonregular-emitting region should be built into the model for further accurate calculation.

3) Effects of Micro-LED Layer: Based on the construction procedures and proton source shown in Figs. 3 and 4, respectively, Fig. 5 compares the intensity distribution during the layer assembly. The total extraction efficiency (η) indicated in the figures can be obtained by directly integrating the angular intensity distribution $I(\theta)$ of the receiver.

$$\eta = \frac{\int I(\theta)\, d\theta}{P_{MQW}} \tag{2}$$

Fig. 4. Modeling of MQW layer: Emitting region (photon source) is immersed in MQW layer.

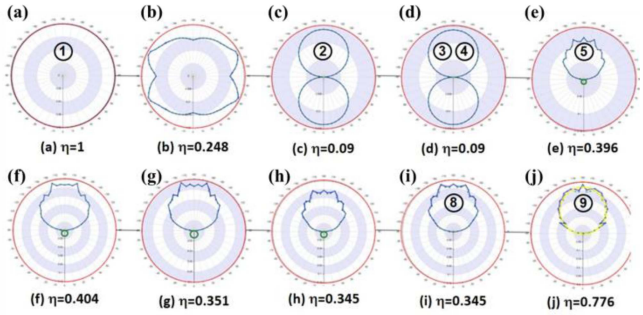

Fig. 5. Intensity distribution variation during layer constructions: (a) MWQ-emitting region, (b) MWQ-emitting region with refractive index (n) = 0.24, (c) MWQ-emitting region immersed in MWQ layer, (d) +P-GaN, (e) +N-GaN, (f) –P-GaN, (g) +N-GaN buffer + Ohmic Region, (h) +P-GaN, (i) +ITO, and (j) +sapphire.

The micro-LED parameter can be slightly adjusted to generate a Lambertian-like intensity distribution after various transformations between the epitaxial layers, indicating that a proper geometric setting can result in better photon extraction from the MQW layer. Note that the receiver of the intensity distribution measurement shown in Fig. 5 is not a conventional far-field receiver, but a finite radius receiver to measure the intrinsic properties of the micro-LED pixel. The next section explains this in detail.

The bins number for the intensity receiver is 51 by 51, whereas the initial number of rays is 50000 k. Additional rays may be emitted depending on the signal-to-noise ratio (S/N) ratio of the receivers to ensure that the S/N ratio $< 5\%$ is an acceptable simulation run for each model. The previous section introduced the Fresnel number $F = \sim 13$, and indicated that the geometric ray tracing is an acceptable strategy for this investigation, such that the FDTD (Finite Difference Time Domain) scheme is not required herein.

4) Radius Settings for Finite Receivers: The following arguments reveal the required modeling setting for the pixel design purpose, especially in the optical interface representing the dramatic in the boundary conditions. Considering a micro-LED array, no accurate intensity distribution measurement exists for a single pixel in the near field, nor is a correct far-field angular apodization (*i.e.*, intensity distribution). The followings are the rationale for this argument.

Fig. 6(a) shows the schematic of the conventional far-field receiver method with a tube-like substrate region below a single pixel (or above, depending on the micro-LED emitting type). However, modeling the substrate as a tube with a far-field receiver produces incorrect boundary conditions on all four sides of the surfaces (nonexistent environment–substrate interface),

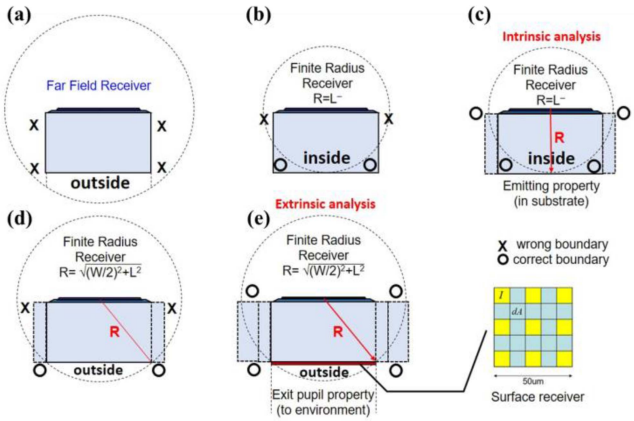

Fig. 6. Setting of receivers and extended pseudo material for single pixels.

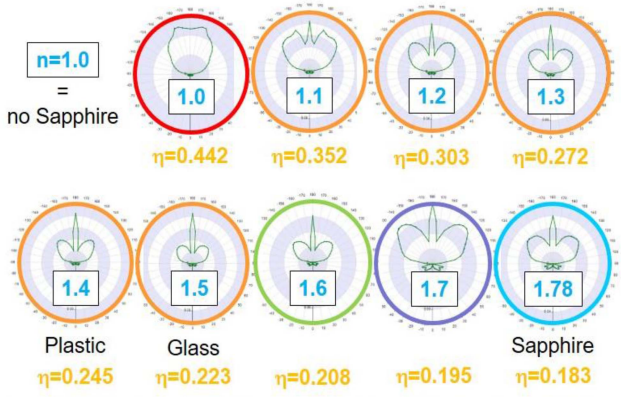

Fig. 7. Conventional far-field simulation results with variation in substrate refractive index (n).

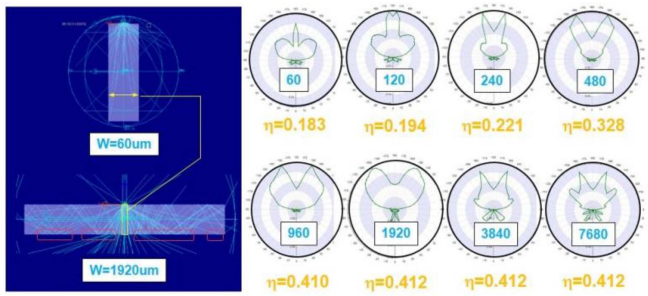

Fig. 8. Intensity distribution by conventional far-field receiver does not converge with extended substrate width from 60–7680 um due to TIR and inappropriate boundary conditions.

which is marked with an "X" symbol. The bottom surface (exit pupil) must be considered; the corner of the substrate also suffers from an incorrect substrate–environment boundary condition. Consequently, this far-field receiver inappropriately records the pixel-based intensity distribution. To overcome this limitation, Fig. 6(b) is converted to a finite radius strategy to solve part of the boundary conditions. However, some problems still exist at some portions of the four sides, so introducing a pseudo environment–substrate interface is required. Thus, Fig. 6(c) demonstrates the extension of the substrate material to ensure the continuity of n within the radius of the finite receiver.

To date, Fig. 6(c) is suitable for evaluating the properties of the intensity distribution of the micro-LED-emitting core by setting the radius of the finite receiver as the length of the substrate. This configuration can record the intrinsic intensity distribution between the layer structures and various etching angles. Recall that Fig. 5(j) was obtained exactly by setting the finite radius in this scenario, thereby considering only the photons emitting distributions inside the pixel structure from the MWQ and through all layers. Considering only the interior structural design is useful, as the environmental material or packaging affects the emission patterns that should not be predestined as the initial design.

Furthermore, to explore the extrinsic properties of the photon emission to the environment (*e.g.*, to the color conversion material, packaging, or air), the setup on a finite radius of the receiver as the diagonal length of the sapphire below the pixel is required: the radius of the finite receiver is enlarged from $R = L$ into $R = ((W/2)^2 + L^2)^{1/2}$ (Fig. 6(d)). However, again, such an arrangement produces incorrect boundary conditions. To solve this problem, again, the extended substrate material strategy is adopted (Fig. 6(e)).

5) Extended Pseudo Material and Environmental Conditions: The arguments in the previous section conclude that if the material is not extended for the specific pixel, nonexistent interfacial refraction occurs. However, if the radius of the receiver is inaccurate, then extending the materials causes undesired TIR and refraction in the bottom surface of the substrates. Fig. 7 demonstrates the far-field distribution (configuration in Fig. 6(a)) that investigators might be interested in the effect of the substrate's n-value. Also, Fig. 8 shows the failure of the extended material that uses the far-field receiver without the correction by the finite radius receiver.

First, the substrate's n-value gradually changes from 1 (air) to 1.78 (sapphire) (Fig. 7). Thus, the peak separation evolution due to Snell's law is evident. If the material is not extended for this measured pixel, the nonexistent interfacial refraction occurs and causes a side emission. Therefore, it is reasonable to confirm the effects of the extended substrate material and check the far-field convergence on the intensity distributions to prove that the self-consistency of the extended substrate can overcome the boundary condition problem. However, in Fig. 8(considering substrate as sapphire with $n = 1.78$), the intensity distribution in the conventional far-field receiver does not converge by doubling the width of the substrates due to the false refraction and TIR problems.

The following is the summary of the scheme for providing the appropriate intensity distribution and illumination measurement in the exit pupil of micro-LED pixels. These are the essential tasks for correcting the pixel-based crosstalk and efficiency evaluation and the guidance for the optimization procedures. The key features of this scheme include setting an appropriate finite receiver radius with the extended substrate to prevent the false TIR and refraction phenomena on the four sides. The radius of the finite receiver is determined by evaluating the intrinsic or extrinsic properties. Care must be taken to ensure the continuity between the layered interfaces. Table I briefly summarizes this scheme.

TABLE I
SUMMARY OF RECEIVER AND EXTENDED MATERIAL SCHEME

- **Interface conditions**
  - Interface between layers
    - top & bottom surface
      - cemented (perfect glue)
      - perfect alignment
  - Interface for pixel boundaries
    - extend the substrate material to meet finite radius receiver
    - four side surfaces
      - specific transmittance
      - TIR & refractive
        - finite radius receiver prevent unrealistic TIR & refraction
    - microLED exit pupil (bottom surface for sapphire | extended substrate)
- **Receiver**
  - finite receiver radius R
    - intrinsic properties
      - finite radius R=L
    - extrinsic properties
      - finite radius $R=(W^2+L^2)^{1/2}$

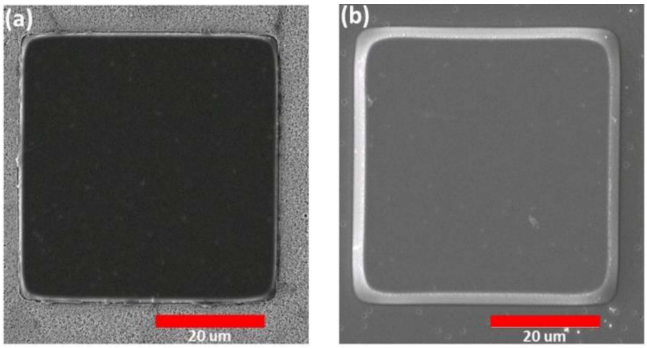

Fig. 9. Comparison of SEM images (top view) of micro-LED ITO/P-GaN/MQW mesa (a) Before and (b) After surface improvement process.

6) SEM Images for Boundary Conditions: To date, the inference for the present methodologies includes a fundamental postulate that the TIR occurs in the interface between the layers. The important clarification for the simulation is to determine whether the real interface can be modeled by the optical software according to this hypothesis. Fig. 9 shows the top-view SEM images of the mesa of the μ-LED chip. In Fig. 9(a), the mesa (ITO/P-GaN/MQW) was fabricated using an inductively coupled plasma etcher with reactive chlorine gases. The impurities are on the N-GaN surface around the mesa. Previous studies have reported that the serious surface roughness is mainly attributed to the etching accumulation, which causes an uneven etch rate phenomenon [14], [15]. In Fig. 9(b), introducing argon during etching improves the etching rate and eliminates the redundant impurities on the N-GaN material. Moreover, it can smoothen the mess-sidewall.

Furthermore, the cross-section shown in Fig. 10 suggests that this smooth interface makes the TIR assumption between the layer surfaces acceptable.

C. Summary

The preceding sections provide the rationale for modeling the micro-LED pixel-based analysis. The construction of layers and effects are demonstrated, and a sufficient reason for using finite radius receivers with extended substrate material to remove the false refraction/TIR boundary conditions is addressed. The configuration for analyzing the intensity of the intrinsic and extrinsic pixels is provided. Fig. 11 reveals the significant difference in the intensity distribution of the micro-LED between the conventional far-field and extrinsic finite field receivers.

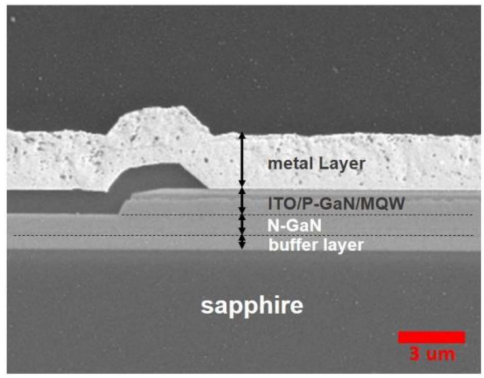

Fig. 10. Cross-sectional SEM image of epitaxial layers.

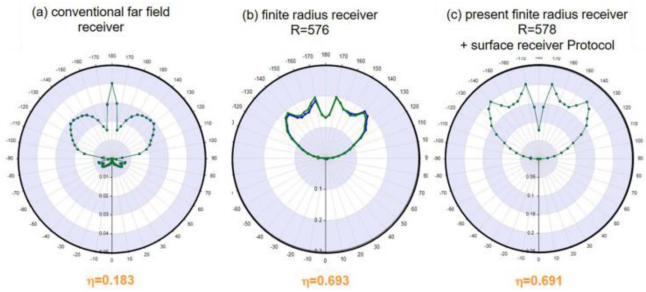

Fig. 11. (a) Far-field receiver without extended material, (b) Finite radius receiver with extrinsic configurations, and (c) Present finite radius receiver.

Fig. 12. Effect of sapphire length (L = 600–50 um) on intensity distribution.

Fig. 12 illustrates the sapphire length effect using the suggested extrinsic configuration. The intensity distribution variance changes significantly under a critical sapphire length (L_C = 300 um). The theoretical study of the critical length and other micro-LED parameters will greatly assist the manufacturer, as it may provide the process tolerance. Note that the efficiency, defined as the integration of the intensity distribution integration, follows the exponential law revealed in Fig. 13. To explore more effects on the micro-LED parameters, the design of experiment (DOE) method [16] is more effective.

D. L_{18} Table for DOE Analysis

The DOE method is appropriate for exploring the critical factors of the micro-LED structure that significantly impact the

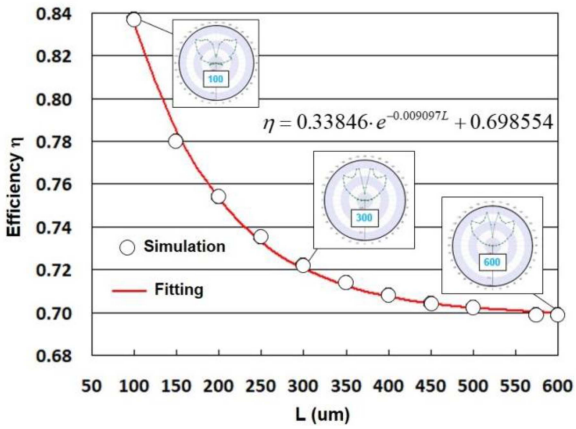

Fig. 13. Efficiency (η) as a function of sapphire length follows the exponential law.

TABLE II
FACTORS AND LEVELS FOR L_{18} TABLE

Factor	Symbol	Notes	Level 1	Level 2	Level3	units
A	L	thickness of sapphire substrate	575	150	-	um
B	a	etching angle of N-GaN layer	21.8°	3.7°	90°	degree
C	b	etching angle of MQW/P-GaN/ITO	48.9°	32.56°	40°	degree
D	p	thickness of P-GaN layer	0.4	0.05	0.5	um
E	h	thickness of buffer layer	1.55	0	0.9	um
F	n	refractive index of extended plate	1.78	1.45	1.57	-
G	T	thickness of extended plate	0	200	100	um
H	t	thickness of ITO layer	0.28	0.15	0.3	um

Exp.1	A	B	C	D	E	F	G	H
1	1	1	1	1	1	1	1	1
2	1	1	2	2	2	2	2	2
3	1	1	3	3	3	3	3	3
4	1	2	1	1	2	2	3	3
5	1	2	2	2	3	3	1	1
6	1	2	3	3	1	1	2	2
7	1	3	1	2	1	3	2	3
8	1	3	2	3	2	1	3	1
9	1	3	3	1	3	2	1	2
10	2	1	1	3	3	2	2	1
11	2	1	2	1	1	3	3	2
12	2	1	3	2	2	1	1	3
13	2	2	1	2	3	1	3	2
14	2	2	2	3	1	2	1	3
15	2	2	3	1	2	3	2	1
16	2	3	1	3	2	3	1	2
17	2	3	2	1	3	1	2	3
18	2	3	3	2	1	2	3	1

specific design target. Here, factors with levels and S/N are discussed in detail in this micro-LED design with an extrinsic finite field receiver scheme.

1) Factors and Levels: In Fig. 1, eight factors are introduced to represent the design factors of the micro-LED. These factors are the substrate thickness (A, sapphire), the etching angle of the N-GaN layer (B), the etching angle of the MQW layer (C, the P-GaN and ITO layers), the N-GaN layer thickness (not a DOE factor, and remains constant as 1.42 um), the P-GaN layer thickness (D), the thickness of the buffer layer (E, between the substrate and the N-GaN layers), the *n*-value of an additional attached substrate (F, if required), the correspondence of the substrate thickness (G), and the ITO layer thickness (H).

Table II summarizes the factors (with symbols) and corresponding numerical values of the levels. Note that there are only two levels for the sapphire substrate thickness, whereas there are three levels for all other factors. This arrangement can lead to an L_{18} DOE Table. During the analysis, the buffer layers between the N-GaN layer and the substrate are assigned as individual entities. If this layer is removed during analysis, one can simply set the material properties to the substrate or the N-GaN layer. According to the number of factors and levels, the L_{18} table for the DOE is introduced. Here, the emphasis is that the combination of level 1 (Exp. #1) is exactly the fabricated micro-LED sample [6].

2) Illuminating Uniformity on Exit Pupil and Extraction Power Efficiency: The η-value for micro-LEDs is important, but

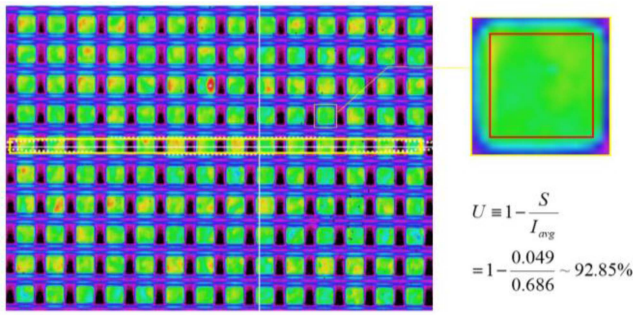

Fig. 14. Measured illuminating condition in exit pupil of micro-LED.

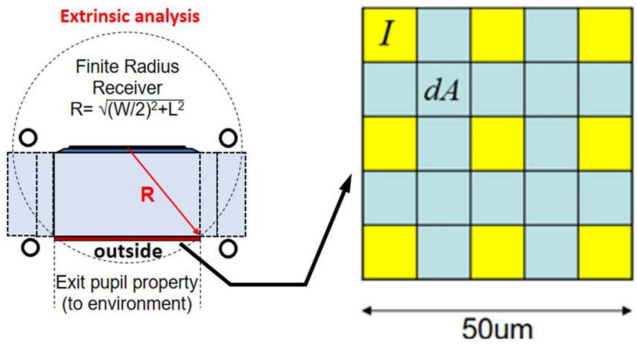

Fig. 15. Surface receiver with 5 × 5 grids for pixel metric measurements.

herein, the luminous power in the normal direction of a single micro-LED pixel exit pupil and the corresponding uniformity are the two principal properties. The merit function construction for the analysis is explained here.

Recall that the configurations in Fig. 6(e) can evaluate the extrinsic intensity distribution of the micro-LED by an angular receiver. Moreover, to calculate the illumination conditions from the exit pupil of the micro-LED, the surface receiver should be set up close to the exit pupil of the micro-LED. Fig. 14 depicts an image of a single-pixel micro-LED for Exp. #1, measured by a beam profiler system (COHU 6612-1000 + PENTAD STAND-50) with a full-frame progressive scan CCD camera. To assess the details in the exit pupil of the micro-LED, a surface receiver with 5 × 5 grids is constructed (Fig. 15) for pixel metric measurements.

In Fig. 15, the measurement occurs by the nine grids (yellow), and each grid contains the luminous power (I_i). Therefore, the luminous uniformity (U) (uniformity for short) can be calculated as follows:

$$I_{avg} = \frac{\sum_{i=1}^{n} I_i}{n} \tag{3}$$

$$S = \sqrt{\frac{\sum_{i=1}^{n} (I_i - \overline{I})^2}{n-1}} \tag{4}$$

$$U = 1 - \frac{S}{I_{avg}} \tag{5}$$

where I_{avg} is the average luminous power, S is the standard deviation, and U is the uniformity. Note that other uniformity

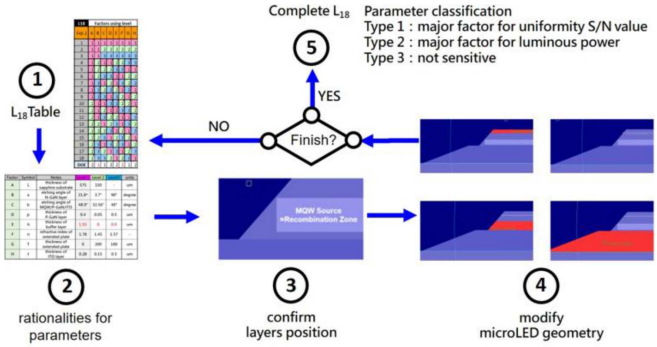

Fig. 16. DOE analysis procedures.

definitions will meet the specific purposes. Although this definition of uniformity is feasible, a more pragmatic way is to introduce the related S/N for the DOE analysis, which has a more dynamic range.

Here are some comments on the pixel based comparison between the measurements and the simulation. It is difficult to measure the intensity distribution of a single pixel micro-LED with proper boundary conditions. This type of measurement requires a sufficient amount of accumulated energy for intensity distribution through the incorporation of several micro-LEDs in a specific region. However, the illuminance uniformity of a single pixel can be identified using the imaging sensors. Consequently, it is more practical to compare the measured relative illumination uniformity with simulation for a single pixel.

The recorded illuminance of the micro-LED display shown in Fig. 14 is based on the following conditions: sapphire substrate thickness = 575 um, N-GaN layer etching angle = 21.8°, MQW layer etching angle = 48.9°, N-GaN layer thickness = 0.9 um, and P-GaN layer thickness = 1.4 um. The refractive index n and the extended plate thickness T are 1.78 and 0 um, respectively. Finally, the ITO layer thickness is 0.28 um. The typical measured average uniformity from the micro-LED array is approximately around 92.85%, which is smaller the simulated intensity distribution (99.63%) from the single pixel in simulation. This measurement error (∼6.8%) might be attributed to the variations during pixel operating.

3) S/N and L_{18} Table: To maximize the luminous power and the exit pupil uniformity of the micro-LED as the major task herein, the L_{18} table was filled using the following S/N definition [17] for "the higher, the better" scenario on I_{avg} with the balancing uniformity.

$$S/N \equiv -10\log_{10}\left(\frac{\sum_{i-1}^{n}\frac{1}{I_i^2}}{n}\right) \sim -10\log_{10}\left(\frac{1}{I_{\text{avg}}^2}\left(1+\frac{3S}{I_{\text{avg}}^2}\right)\right) \quad (6)$$

Fig. 16 presents the complete procedures for analyzing the essential factors influencing the extrinsic properties the most for the luminous power and uniformity in the exit pupil of the micro-LED. Recall that in the successive construction of the micro-LED layer structure, care must be taken for the continuity of the surfaces and the compatibility between the geometric form factors and the material and surface properties of the layer

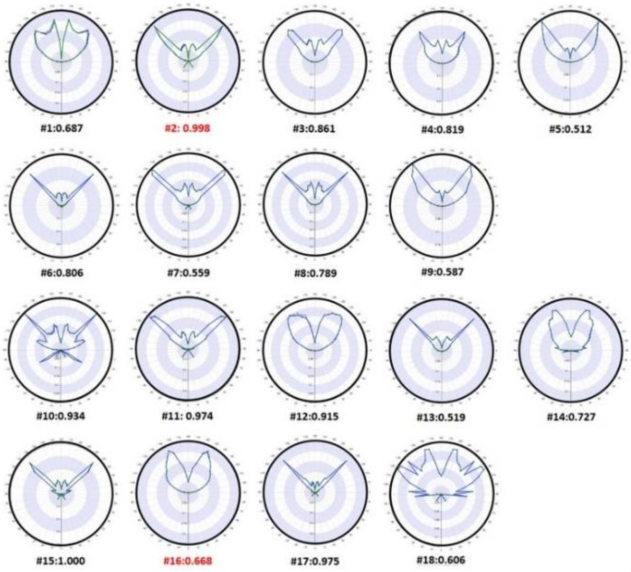

Fig. 17. Intensity distribution for L_{18} experiments.

region. In the following section, the sensitivity for the uniformity and the luminous power, as well as the correlation between these metrics, will be addressed to guide the categories of major factors and optimum design strategies for micro-LEDs.

III. Results and Discussion

The following subsections investigate the major factors of the total luminous power and the uniformity of the surface receivers. Also, the intensity distributions for experimental configurations (according to the finite radius extrinsic analysis scheme) are revealed.

A. Results of L_{18} Table

Table III presents the complete analysis results for the L_{18} experiments. The luminous power on the measured grids (I_{i}), I_{avg}, S, S/N for the larger, the better $S/N_{\max}$, and related metrics, such as U and η, are presented as well. Note that for #15, η is adjusted to the upper limit due to the possible integral scheme error. The complete intensity distribution (extrinsic finite receiver scheme) for different factor configurations is presented in Fig. 17. Table III Results of L_{18} table.

These distributions form an analysis basis set for evaluating the sensitivities between the factors. Note that for some designs, the maximum intensity occurs at a particular angle. However, whether or not these intensities will result in pixel crosstalk is determined by the geometric arrangements between the pixels and the observation configurations.

B. Sensitivity to Luminous Power and Uniformity

Following the DOE procedures, the sensitivity analysis presented in Table IV and Fig. 18 provides a detailed ranking of all design factors for the luminous power by considering I_{avg}. Evidently, three major factors significantly influence the luminous power on the surface receiver set up in the exit pupil. These are factors A (sapphire thickness), D (P-GaN layer thickness),

TABLE III
RESULTS OF L_{18} TABLE

L18	Level for Factors								Measurements									Analysis					
Exp.1	A	B	C	D	E	F	G	H	I1	I2	I3	I4	I5	I6	I7	I8	I9	Average	S	S/N Max	Approx	U	η
1	1	1	1	1	1	1	1	1	4.25	4.26	4.21	4.24	4.26	4.24	4.23	4.22	4.24	4.24	0.018	12.543	12.531	99.63%	0.687
2	1	1	2	2	2	2	2	2	2.68	2.67	2.67	2.67	2.67	2.67	2.70	2.66	2.67	2.67	0.010	8.541	8.523	99.71%	0.998
3	1	1	3	3	3	3	3	3	3.28	3.31	3.31	3.31	3.36	3.33	3.25	3.32	3.28	3.31	0.034	10.386	10.347	99.19%	0.861
4	1	2	1	1	2	2	3	3	4.83	4.90	4.85	4.85	4.90	4.88	4.80	4.88	4.83	4.86	0.034	13.726	13.708	99.44%	0.819
5	1	2	2	2	3	3	1	1	5.15	5.27	5.15	5.23	5.41	5.27	5.13	5.25	5.06	5.21	0.105	14.340	14.294	98.41%	0.512
6	1	2	3	3	1	1	2	2	2.99	2.98	2.98	2.98	3.02	3.03	3.00	2.99	3.01	3.00	0.020	9.538	9.510	99.43%	0.806
7	1	3	1	2	1	3	2	3	2.33	2.29	2.28	2.34	2.31	2.31	2.32	2.33	2.33	2.31	0.017	7.284	7.242	99.34%	0.559
8	1	3	2	3	2	1	3	1	5.11	5.17	5.09	5.18	5.25	5.18	5.06	5.17	5.07	5.14	0.062	14.219	14.191	99.07%	0.789
9	1	3	3	1	3	2	1	2	6.23	5.71	6.23	5.84	5.33	5.85	6.39	5.85	6.29	5.97	0.343	15.477	15.394	95.37%	0.587
10	2	1	1	3	3	2	2	1	9.32	9.28	9.31	9.29	9.26	9.29	9.33	9.27	9.30	9.30	0.023	19.366	19.362	99.81%	0.934
11	2	1	2	1	1	3	3	2	20.97	20.86	21.02	20.80	20.71	20.89	20.94	20.83	20.97	20.89	0.098	26.397	26.395	99.62%	0.974
12	2	1	3	2	2	1	1	3	49.60	50.61	49.61	50.54	51.63	50.63	49.55	50.61	49.66	50.27	0.711	34.024	34.023	98.90%	0.915
13	2	2	1	2	3	1	3	2	32.28	31.51	32.31	31.57	30.75	31.52	32.26	31.50	32.33	31.78	0.547	30.039	30.036	98.65%	0.519
14	2	2	2	3	1	2	1	3	70.97	72.39	71.19	72.15	73.74	72.20	70.56	72.08	70.63	71.77	1.025	37.116	37.116	98.87%	0.727
15	2	2	3	1	2	3	2	1	16.71	16.65	16.69	16.62	16.58	16.61	16.60	16.61	16.65	16.64	0.043	24.421	24.419	99.80%	1.000
16	2	3	1	3	2	3	1	2	81.79	84.74	81.68	84.78	88.32	84.69	82.40	85.22	82.43	84.01	2.152	38.479	38.482	97.99%	0.668
17	2	3	2	1	3	1	2	3	15.04	15.69	15.05	15.61	16.39	15.69	14.79	15.55	14.84	15.41	0.519	23.741	23.726	97.36%	0.975
18	2	3	3	2	1	2	3	1	17.71	17.09	17.63	17.31	16.71	17.24	17.85	17.28	17.73	17.40	0.367	24.803	24.793	98.30%	0.606

TABLE IV
RANKING OF MAJORS FACTORS FOR LUMINOUS POWER ON SURFACE RECEIVER

Factor / values / terms	A	B	C	D	E	F	G	H
Level 1	4.079	15.112	22.748	11.332	19.933	18.306	36.911	9.653
Level 2	35.272	22.209	20.182	18.274	27.264	18.660	8.221	24.719
Level 3		21.705	16.096	29.419	11.829	22.060	13.894	24.654
E12	31.192	7.097	-2.566	6.942	7.330	0.354	-28.690	15.065
E23		-0.504	-4.086	11.145	-15.435	3.401	5.674	-0.065
Max	35.272	22.209	22.748	29.419	27.264	22.060	36.911	24.719
Min	4.079	15.112	16.096	11.332	11.829	18.306	8.221	9.653
Range	31.192	7.097	6.652	18.087	15.435	3.755	28.690	15.065
Rank	1	6	7	3	4	8	2	5
Singnificant	1			3			2	

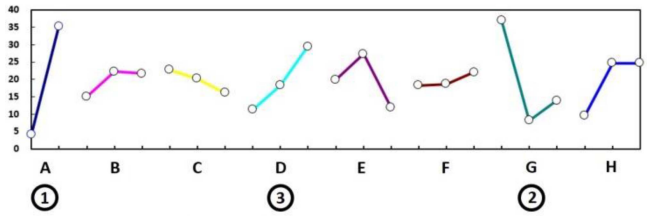

Fig. 18. Ranking of major factors for luminous power.

TABLE V
RANKING OF MAJOR FACTORS FOR LUMINOUS POWER UNIFORMITY

Factor / values / terms	A	B	C	D	E	F	G	H
Level 1	11.784	18.543	20.240	19.384	19.614	20.684	25.330	18.282
Level 2	28.710	21.530	20.726	19.839	22.235	19.838	15.482	21.412
Level 3		20.667	19.775	21.517	18.892	20.218	19.929	21.046
E12	16.926	2.987	0.486	0.454	2.621	-0.846	-9.848	3.130
E23		-0.863	-0.951	1.679	-3.343	0.379	4.447	-0.366
Max	28.710	21.530	20.726	21.517	22.235	20.684	25.330	21.412
Min	11.784	18.543	19.775	19.384	18.892	19.838	15.482	18.282
Range	16.926	2.987	0.951	2.133	3.343	0.846	9.848	3.130
Rank	1	5	7	6	3	8	2	4
Singnificant	1				3		2	

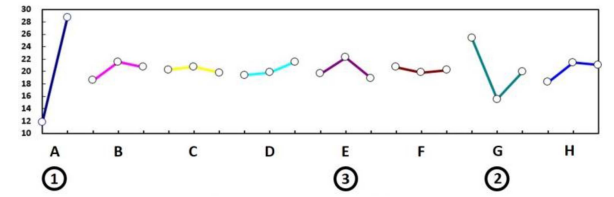

Fig. 19. Ranking of major factors for luminous power uniformity.

and G (extended plate thickness). The S/N range in factor A is 31.192, and is $>$ the interaction design parameter, such as factor C (S/N range $= 6.652$, etching angle of the MQW layer). The design factors can be the concentrated optimization in the commercial design and fabrication process, which can be applied to the cost control of micro-LED displays. Notice that there are turning points on factor E (buffer layer thickness) and factor G (extended plate thickness) for the level provided in the DOE.

In contrast, Table V and Fig. 19 rank all design factors for the luminous power uniformity, which is characterized by S/N. Similar analysis procedures reveal that three factors affect the exit pupil uniformity: factors A (sapphire thickness), E (buffer layer thickness), and G (extended plate thickness). Factors A and G are the major factors improving the luminous power and uniformity since their S/N values are the top two in Tables IV and V.

In designing color conversion micro-LED full-color displays, the illuminance uniformity and efficiency are the essential performance characteristics [10], [18], which can be further optimized by factors A and G. Hence, factors A and G (sapphire and the extended plate thicknesses), together as a generalized substrate structure, are the two critical factors for improving the design qualities of the luminous power and the uniformity of the micro-LED light extraction for these bottom emitting configurations.

C. Categories for Major Factors and Optimum Design Strategies

Through analysis, these eight factors can be classified into three categories: group 1 (factors A, D, and G) for increasing the luminous power, group 2 (factors A, E, and G) for increasing the luminous power uniformity, and group 3 (factors B, C, F, and H) for decreasing the factory overheads. First, the initial optimum design can be approach by maximizing the luminous

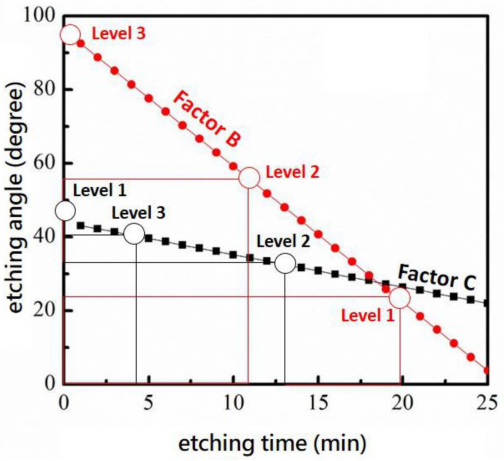

Fig. 20. Relationship between etching time and angle for factors B and C.

power through group 1. Next, the luminous power uniformity is adjusted using the group 2 parameters. A trade-off is expected between factors A and G in case of luminous power and uniformity, and factor E (buffer layer thickness) might be able to accommodate part of these inconsistencies. Further investigation on the etching angle effects of the N-GaN layer (B), etching angle of the MQW/P-GaN/ITO layer compound (C), the *n*-value of an additional attached substrate (F), and the ITO layer thickness (H) is important. These factors (group 3) can be used to modify the intensity distribution and reduce the steps involved in the manufacturing process.

Fig. 20 shows the etching time for factors B (angle of the N-GaN layer) and C (angle of the MQW/P-GaN/ITO layer compound). Because the etching angle is less sensitive to the luminous power and uniformity, here, a minimum etching angle is sufficient to meet the design objective. To reduce the discontinuous coverage of metal contact in the micro-LED array-chip structure, the tapered sidewall of the N-GaN and MQW/P-GaN layers can be designed at a smaller angle without altering the optical properties. However, concerning the electrical properties, the metal contact arrays can provide smoother coverage on the chip and reduce the series resistance [6].

IV. Conclusion

Here, the protocol for numerical modeling micro-LED pixels is presented in detail. The successive construction of the pixel structures, including the sapphire substrate, the N-GaN layer, the MQW layer, the P-GaN layer, the ITO contact, and the refractive index (*n*) of an additional attached substrate, have been successively constructed step-by-step manner to ensure the cemented surface and immersion options can propagate the photon continuity in the interface. We have effectively rectified the configuration errors in common LED optical simulations.

The far-field receiver has been proved incorrect for the pixel base analysis, such that extending the substrate material to avoid false side effects is essential. Therefore, a finite-radius receiver rather than a far-field receiver is a more pragmatic approach and introduces the finite receiver radius concept for intrinsic and extrinsic measurements. Based on the correct measurement tool, the DOE L_{18} table identifies the major factors for luminous power and uniformity on the pixel exit pupil.

The further optimization strategies are guided by the variations of the intensity distributions under different configurations. The optimal uniformity of 99.81% can be obtained using the following optimal factors: sapphire substrate thickness = 150 um; etching angle of the N-GaN layer = 21.8°; etching angle of the MQW layer = 48.9°; thickness of the N-GaN layer = 0.9 um; thickness of the P-GaN layer = 1.4 um; n-value = 1.45; thickness of the extended plate = 200 um; and thickness of the ITO layer = 0.28 um. This uniformity is suitable for designing full-color micro-LED displays.

References

[1] Z. Chen, S. Yan, and C. Danesh, "MicroLED technologies and applications: Characteristics, fabrication, progress, and challenges," *J. Phys. D: Appl. Phys.*, vol. 54, 2021, Art. no. 123001, doi: 10.1088/1361-6463/abcfe4.

[2] P. J. Parbrook, B. Corbett, J. Han, T.-Y. Seong, and H. Amano, "Micro-light emitting diode: From chips to applications," *Laser Photon. Rev.*, vol. 15, 2021, Art. no. 2000133, doi: 10.1002/lpor.202000133.

[3] C.-C. Lin, K.-L. Liang, W.-H. Kuo, H.-T. Shen, C.-I. Wu, and Y.-H. Fang, "Colloidal quantum dot enhanced color conversion layer for micro LEDs," *IEICE Trans. Electron.*, vol. 105, pp. 52–58, 2021, doi: 10.1587/transele.2021DII0005.

[4] J. Park et al., "Electrically driven mid-submicrometre pixelation of InGaN micro-light-emitting diode displays for augmented-reality glasses," *Nature Photon.*, vol. 15, pp. 449–455, 2021, doi: 10.1038/s41566-021-00783-1.

[5] A. M. Noor Elahi and J. Xu, "Electrical and optical modeling of gap-free III-nitride micro-LED arrays," *AIP Adv.*, vol. 10, 2020, Art. no. 105028, doi: 10.1063/5.0027809.

[6] P.-W. Chen et al., "Improved performance of passive-matrix micro-LED displays using a multi-function passivation structure," *IEEE Photon. J.*, vol. 12, no. 4, Aug. 2020, Art no. 7000711, doi: 10.1109/JPHOT.2020.3002554.

[7] F. Gou et al., "Angular color shift of micro-LED displays," *Opt. Exp.*, vol. 27, pp. A746–A757, 2019, doi: 10.1364/OE.27.00A746.

[8] W. Betty, "Sundiode achieves full-color micro-displays based on stacked 3-color micro-LEDs, semiconductor today," Nov. 9, 2021. [Online]. Available: https://www.ledinside.com/node/32409

[9] Z. T. Ye and J.-Y. Wu, "Use of recycling-reflection color-purity enhancement film to improve color purity of full-color micro-LEDs," *Nanoscale Res. Lett.*, vol. 17, no. 1 pp. 1–10, Dec. 2022, doi: 10.1186/s11671-021-03642-8.

[10] Y. Wu, J. Ma, P. Su, L. Zhang, and B. Xia, "Full-color realization of micro-LED displays," *Nanomaterials*, vol. 10, 2020, Art. no. 2482, doi: 10.3390/nano10122482.

[11] F. J. Bruni, "Crystal growth of sapphire for substrates for high-brightness, light emitting diodes," *Cryst. Res. Technol.*, vol. 50, pp. 133–142, 2015, doi: 10.1002/crat.201400230.

[12] J. W. Goodman, *Introduction to Fourier Optics*, 2nd ed. New York, NY, USA: McGraw Hill, 1996.

[13] Z. Wang, X. Shan, X. Cui, and P. Tian, "Characteristics and techniques of GaN-based micro-LEDs for application in next-generation display," *J. Semicond.*, vol. 41, 2020, Art. no. 041606, doi: 10.1088/1674-4926/41/4/041606.

[14] S. A. Rosli, A. A. Aziz, and M. R. Hashim, "ICP-RIE dry etching using Cl_2-based on GaN," *Sains Malaysiana*, vol. 40, no. 1, pp. 79–82, 2011.

[15] X. Guo and E. F. Schubert, "Current crowding and optical saturation effects in GaInN/GaN light-emitting diodes grown on insulating substrates," *Appl. Phys. Lett.*, vol. 78, pp. 3337–3339, 2001, doi: 10.1063/1.1372359.

[16] Department of Mathematics, University of York, Orthogonal Arrays (Taguchi Designs), Apr. 7, 2022. [Online]. Available: https://www.york.ac.uk/depts/maths/tables/orthogonal.htm

[17] N. Belavendram., *Quality by Design: Taguchi Techniques for Industrial Experimentation*. Hoboken, NJ, USA: Prentice Hall, 1995.

[18] Y.-M. Huang et al., "High-uniform and high-efficient color conversion nanoporous GaN-based micro-LED display with embedded quantum dots," *Nanomaterials*, vol. 11, 2021, Art. no. 2696, doi: 10.3390/nano11102696.